JACS
JOURNAL OF THE AMERICAN CHEMICAL SOCIETY

ARTICLE

pubs.acs.org/JACS

Non-covalent Monolayer-Piercing Anchoring of Lipophilic Nucleic Acids: Preparation, Characterization, and Sensing Applications

Moria Kwiat,[†,#] Roey Elnathan,[†,#] Minseok Kwak,[⊥] Jan Willem de Vries,[⊥] Alexander Pevzner,[†] Yoni Engel,[†] Larisa Burstein,[‡] Artium Khatchtourints,[§] Amir Lichtenstein,[†] Eli Flaxer,[†] Andreas Herrmann,[*,⊥] and Fernando Patolsky[*,†]

[†]School of Chemistry, Raymond and Beverly Sackler Faculty of Exact Sciences, [‡]Wolfson Applied Materials Research Center, and [§]The Center for Nanoscience and Nanotechnology, Tel Aviv University, Tel Aviv 69978, Israel

[⊥]Zernike Institute for Advanced Materials, Department of Polymer Chemistry, University of Groningen, Nijenborgh 4, 9747 AG Groningen, The Netherlands

Supporting Information

ABSTRACT: Functional interfaces of biomolecules and inorganic substrates like semiconductor materials are of utmost importance for the development of highly sensitive biosensors and microarray technology. However, there is still a lot of room for improving the techniques for immobilization of biomolecules, in particular nucleic acids and proteins. Conventional anchoring strategies rely on attaching biomacromolecules via complementary functional groups, appropriate bifunctional linker molecules, or non-covalent immobilization via electrostatic interactions. In this work, we demonstrate a facile, new, and general method for the reversible non-covalent attachment of amphiphilic DNA probes containing hydrophobic units attached to the nucleobases (lipid−DNA) onto SAM-modified gold electrodes, silicon semiconductor surfaces, and glass substrates. We show the anchoring of well-defined amounts of lipid−DNA onto the surface by insertion of their lipid tails into the hydrophobic monolayer structure. The surface coverage of DNA molecules can be conveniently controlled by modulating the initial concentration and incubation time. Further control over the DNA layer is afforded by the additional external stimulus of temperature. Heating the DNA-modified surfaces at temperatures >80 °C leads to the release of the lipid−DNA structures from the surface without harming the integrity of the hydrophobic SAMs. These supramolecular DNA layers can be further tuned by anchoring onto a mixed SAM containing hydrophobic molecules of different lengths, rather than a homogeneous SAM. Immobilization of lipid−DNA on such SAMs has revealed that the surface density of DNA probes is highly dependent on the composition of the surface layer and the structure of the lipid−DNA. The formation of the lipid−DNA sensing layers was monitored and characterized by numerous techniques including X-ray photoelectron spectroscopy, quartz crystal microbalance, ellipsometry, contact angle measurements, atomic force microscopy, and confocal fluorescence imaging. Finally, this new DNA modification strategy was applied for the sensing of target DNAs using silicon-nanowire field-effect transistor device arrays, showing a high degree of specificity toward the complementary DNA target, as well as single-base mismatch selectivity.

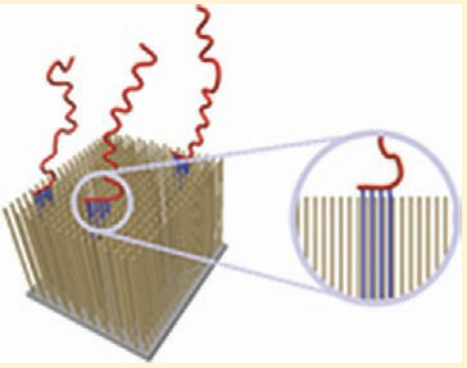

INTRODUCTION

Biofunctional interfaces of biomolecules and solid inorganic substrates (such as semiconductor materials) have been the focus of enormous interest in basic and applied science due to their vast potential applications in fields including proteomics, microarray technology, and biosensors.[1−10] It is anticipated that these hybrid biointerfaces will be able to perform specific functions, such as biorecognition in the context of electrical, mass, and optical measurements, better than either purely organic or inorganic systems.[11−16] For example, on-surface hybridization, in which single-stranded (ss) DNA targets are tethered to a solid support and bind DNA analyte molecules from solution, forms the basis of modern microarray and biosensor DNA biotechnologies extensively used in genotyping, studying gene expression, and biological detection applications.[17−23] DNA chips or DNA microarrays, on which thousands of hybridization reactions are carried out in parallel, are regularly used to address fundamental questions of biology and for clinical and research sample characterization, even on the whole-genome scale. Biomolecule-modified solid surfaces or biosensors are usually dedicated to the specific and quantitative detection of a single or multiple analytes, often performed in real time.[24−28] For such applications, ssDNA oligonucleotide probes are in general covalently immobilized via a functional linker onto the metal or semiconductor surface, directly or mediated by a previously modified

Received: July 20, 2011
Published: November 15, 2011

dx.doi.org/10.1021/ja206639d | J. Am. Chem. Soc. 2012, 134, 280–292

reactive thin organic film.[29] Common approaches for the preparation of DNA monolayers involve the formation of stable sulfur−gold bonds between thiol-derivatized oligonucleotides and Au surfaces[30−33] or the utilization of cross-coupling linker moieties, often carrying maleimide or *N*-hydroxysuccinimide groups, to furnish a proper connection between DNA and siloxane layers.[34−37] Additionally, non-covalent surface modification routes solely based on electrostatic interactions between the negatively charged DNA probe elements and positively charged surfaces have been demonstrated.[38,39] In spite of their frequent use, these approaches do not offer a satisfactory degree of control over the basic attributes required for most sensing purposes.

Nucleic acid sensing employing DNA probe layers requires that hybridization capability and specificity be maintained and that non-specific interactions between the solid surface and the DNA target be minimized. These criteria remain the imperative goals for improvements in the sensing performance of DNA biosensor devices. Indeed, the hybridization behavior of probe and complementary target DNA molecules at the solid−liquid interface can differ significantly from the analogous hybridization processes in solution. When base pairing occurs at a solid surface, non-specific probe−surface interactions may represent a critical issue with considerable influence on the efficacy and capacity of DNA hybridization-based sensing devices. In order to reduce non-specific surface adsorption of DNA analyte molecules, as well as the adsorption of other biomolecules that may be present in complex biological samples under inspection, anti-fouling spacer layers such as cellulose, poly(acrylamide), and poly(ethylene glycol) (PEG) have been applied to anchor the DNA probe strands onto solid surfaces.[40] These approaches have been proven effective, but much room for improvement remains in the design of chemical anchoring procedures.

In general, the surface chemistry for the immobilization of DNA and other biomolecules should proceed under mild reaction conditions in aqueous media and under ambient conditions to enable smooth integration with device fabrication. In addition, the passivation layer between the DNA probe molecules and the solid substrate should be as dense as possible to minimize non-specific analyte adsorption effectively and prevent misleading analysis.

Most of the hybrid biointerfaces discussed above are generated as self-assembled monolayers (SAMs). In general, SAMs are highly ordered single layers of organic molecules formed by spontaneous adsorption of an active surfactant onto a solid surface, and they provide a versatile and powerful tool to generate monomolecular films of biological molecules on a variety of surfaces. This technique has developed dramatically in terms of synthetic sophistication and depth of characterization over the past two decades and is now applied for the development of sensing applications because of several attractive features. First, miniaturization is easy due to the minimal resources needed (e.g., a monolayer may contain as few as 10^{13} molecules/cm^2). Second, the simple procedure of SAM formation and its compatibility with solid substrates for electrochemical measurements offer special benefits for biosensor applications. Most importantly, the highly ordered and dense nature of long-chain alkanethiol SAMs mimics the cellular microenvironment of lipid bilayer structures, thus potentially offering novel substrates for immobilization of biomolecules or more complex biological systems. To take full advantage of this potential, these biological species could be compatibilized with the SAM through appropriate chemical modifications.

Broadly, the combination of hydrophobic elements such as long alkyl chains with hydrophilic units leads to amphiphilic species, which are essential building blocks for self-assembled materials. They are capable of forming a variety of structures of different morphology and size, depending on the hydrophobic volume and the size of the headgroup, as well as other variables such as concentration, temperature, pH, and solvent. Many such structures are present in nature and play important roles in biological processes, for instance phospholipids in the bilayers of cell membranes and intracellular vesicles. Some of these self-assembled aggregates have been reproduced *in vitro* and employed as nanoreactors and containers for catalysts as well as for gene and drug delivery.[41−44] A more recent development in this field is the generation of hybrid amphiphiles containing hydrophobic units and hydrophilic biomacromolecule components. In these materials, the biological building blocks are peptides and oligonucleotides, covalently attached to hydrophobic polymers such as poly(propylene oxide) (PPO),[45,46] polystyrene,[47] poly(butyl acrylate), and poly(D,L-lactic-*co*-glycolic acid) (PLGA)[48] or small hydrophobes like linear and branched alkyl chains.[49,50] Among those hybrids, DNA-based materials are especially appealing due to their sequence programmability, self-recognition, and mechanical properties. A common motif for the DNA amphiphiles is terminal functionalization at the sugar−phosphate backbone, for instance with cholesterol[51] or long alkyl chains for anchoring into lipid bilayers.[52]

Here, we demonstrate a new and general method for the reversible non-covalent anchoring of amphiphilic DNA probes containing hydrophobic units attached to the nucleobases (lipid−DNA)[53,54] onto SAM-modified gold electrodes, silicon semiconductor surfaces, and glass substrates. Using hydrophobic SAMs as an anchoring basis, we show the anchoring of well-defined amounts of lipid−DNA onto the surface by piercing their lipid tails into the monolayer structure. The surface coverage of DNA molecules can be controlled by simply modulating the initial concentration and incubation time. Further control over the DNA layer is afforded by the additional external stimulus of temperature. Heating the DNA-modified surfaces at temperatures >80 °C leads to the release of the lipid−DNA structures from the surface without harming the integrity of the hydrophobic SAMs. The DNA-free surface can then be repeatedly modified with lipid−DNA probe molecules in the same manner, which should allow further cycles of nucleic acid sensing and the reuse of analytical devices. These DNA layers can be further tuned by anchoring onto a mixed SAM containing hydrophobic molecules of different lengths, rather than a homogeneous SAM. Immobilization of lipid−DNA on such SAMs has revealed that the surface density of DNA probes is highly dependent on the composition of the surface layer and the structure of the lipid−DNA. The number of lipophilic tails, either two or four in the structures addressed here, is an important parameter influencing the insertion capabilities and the stability of the resulting immobilized DNA layers.

The formation of the lipid−DNA sensing layers was monitored and characterized by X-ray photoelectron spectroscopy (XPS), quartz crystal microbalance (QCM) experiments, ellipsometry, contact angle measurements, atomic force microscopy (AFM), and confocal fluorescence imaging. Finally, this new DNA modification strategy was applied for the sensing of target DNAs using silicon-nanowire field-effect transistor (FET) device arrays, showing a high degree of specificity toward the complementary DNA (cDNA) target, as well as single-base mismatch selectivity.

Scheme 1. General Schematic for the Formation of Lipid−DNA Hybrid-Based Sensing Layers

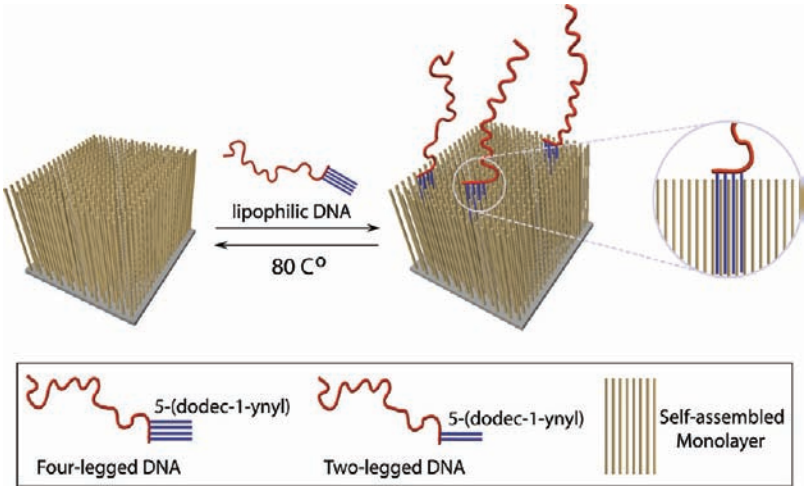

RESULTS AND DISCUSSION

As mentioned above, the major requirements for a nucleic acid sensing device are specific binding of a DNA analyte and promotion of its hybridization onto a surface-tethered DNA probe with minimal non-specific adsorption. The general schematic for the formation of lipid−DNA hybrid-based sensing layers is depicted in Scheme 1. First, a self-assembled hydrophobic monolayer was deposited either onto gold by incubation with an alkanethiol in ethanol solution or onto silicon oxide from a hydrophobic silane derivative in heptane solution. These hydrophobic SAMs served as substrates for the insertion of lipid−DNA molecules. The hydrophobicity was introduced into the oligodeoxyribonucleotides (ODNs) by attaching a dodec-1-yne chain at the 5-position of the uracil base. Solid-phase synthesis allows introduction of this building block at any position in the DNA sequence. Here, two or four modified 2′-deoxyuridines were incorporated at the 5′-end of the ODNs: **U2T** (5′-U*U*TGGCGGATTC-3′, where U* represents modified 2′-deoxyuridine) and **U4T** (5′-U*U*U*U*GCGGATTC-3′), each composed of 12 nucleotides.[53,54] After a dense SAM was formed, the surfaces were incubated with an aqueous solution containing **U2T** or **U4T**. This process led to the non-covalent insertion of the lipid−DNA molecules into the hydrophobic monolayer through the lipophilic tails attached to the DNA (Scheme 1 inset). The resulting DNA-modified surfaces were applied as sensors of DNA analyte molecules in solution. Under heating at 80−100 °C with supernatant solution, the inserted lipid−DNA molecules were extracted from the hydrophobic SAM. The surface could be reactivated with lipid−DNA target molecules through re-insertion by repeated incubation.

To characterize the surface modification, we carried out XPS analysis on silicon wafers after each functionalization step. As shown in Figure 1, these measurements revealed that the modification process induced significant changes in the sample elemental composition, providing clear evidence that the surfaces have been chemically modified. The XPS survey spectrum of the pristine silicon wafers revealed the presence of mainly silicon and oxygen, as well as trace amounts of carbon.

Silicon wafers were first modified by incubation of *n*-octadecyldimethylchlorosilane (C_{18}Si) in heptane solution for different time periods (see Experimental Section for details) until a densely packed SAM was formed. XPS measurements showed a significant increase in the C1s peak from clean Si oxide surface (Figure 1A) to an incubated surface (Figure 1B). Incubation periods ranging from 1 to 48 h showed that after approximately 8 h a plateau of C1s atomic concentration was reached (Figure 1C inset). This behavior strongly indicates the formation of a dense hydrophobic monolayer. Moreover, the results of XPS elemental analysis (Table 1) showed a marked enhancement in the atomic ratio of C/Si for the monolayer-functionalized samples (1:1.9 on average) in comparison to that measured for the unmodified silicon control (1:13.8). This observation provides additional support for the presence of alkylsilane molecules on the surfaces.

Contact angle measurements were also performed on these surfaces (Figure 1D). In general, a surface with a contact angle greater than 90° is designated as hydrophobic. Values of 95° were already achieved after an incubation time of only 1 h, a stark contrast to the contact angle of 42° measured for bare silicon oxide (data not shown). The increase in contact angle clearly proved the formation of a dense hydrophobic monolayer on the silicon wafer surface. Further validation for the formation of a hydrophobic monolayer after 1 h of incubation with C_{18}Si was explored by ellipsometry measurements, which yielded a film thickness of 15.0 ± 0.9 Å.

Subsequently, incubation of the resulting C_{18}Si-SAM with a 1 μM aqueous solution of **U4T** for different periods of time led to a clear increase in the C1s and N1s peaks, consistent with the expected addition of carbon and nitrogen components originating from the inserted lipid−DNA molecules (Figure 2A,B). Longer incubation times led to higher atomic concentrations of these elements, as expected, up to a period of ∼20 h. Also, contact angle measurements show a distinct reduction of contact angle upon **U4T** insertion, further demonstrating the successful functionalization of the surface (Figure 2D). In addition, ellipsometry measurements confirm the insertion of **U4T** into the hydrophobic monolayer by an evident increase in the height to 30.8 ± 0.6 Å (∼100% increase). As shown in Figure 2C, AFM phase images of a hydrophilic SiO_2 wafer with hydrophobic C_{18}Si-micropatterned squares and lines in which **U4T** lipid−DNA was inserted provide yet another proof of successful anchoring. Namely, there is a change in the phase contrast

dx.doi.org/10.1021/ja206639d | *J. Am. Chem. Soc.* 2012, 134, 280–292

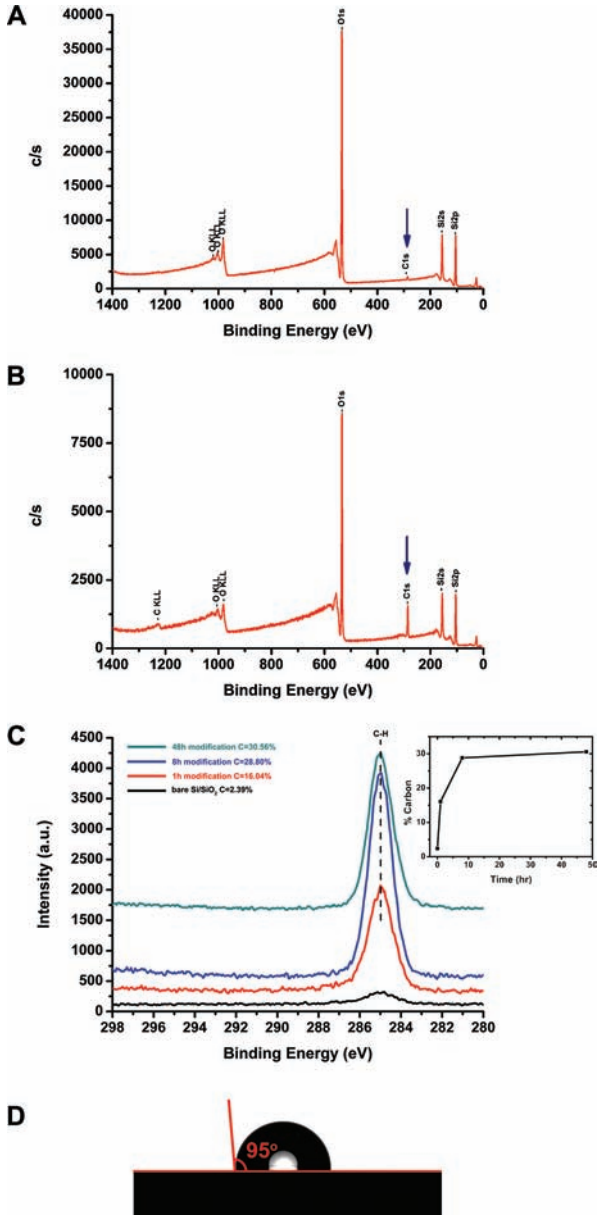

Figure 1. Characterization of the formation of hydrophobic monolayers of *n*-octadecyldimethylchlorosilane ($C_{18}Si$) on Si/SiO_2 wafers. (A) XPS survey spectrum of bare Si oxide substrate. The weak C1s peak is indicated. (B) XPS survey spectrum of the Si oxide substrate chemically modified with $C_{18}Si$, showing an increase in the C1s peak. (C) High-resolution XPS spectra showing C1s peaks of a bare silicon oxide wafer (black) modified with $C_{18}Si$ for periods of 1 (red), 8 (blue), and 48 h (green), revealing a significant increase in the C1s peak upon monolayer formation. Inset: Growth of the C1s peak over time, with a clear plateau after approximately 8 h reaction time. (D) Contact angle measurement showing a value of 95° after 1 h incubation time with $C_{18}Si$, in comparison to a contact angle of 42° for bare silicon oxide, indicating the formation of a hydrophobic monolayer.

between monolayer and substrate as the patterned region shifts from hydrophobic to hydrophilic upon insertion of DNA. Similar experiments were performed using (heptadecafluoro)-1,1,2,2-tetrahydrodecyldimethylchlorosilane to probe the role of surface hydrophobicity. The fluorosilane derivative forms a less hydrophobic monolayer than $C_{18}Si$, as indicated by its lower contact angle of 72°, which resulted in poorer lipid−DNA insertion efficiency (Figure S4).

Lipid−DNA species are presumably incorporated through stabilization of pre-existent defects in the SAMs. This behavior is similar to the reported mechanisms for the exchange of alkanethiol monolayers.[55−57] In the current case, no exchange reaction can take place; instead, the lipophilic tails of lipid−DNA enter and fill defect gaps in the SAM, in this manner stabilizing the whole monolayer structure.

Having successfully realized a lipid−DNA monolayer, we proceeded to evaluate the capacity of tethered **U4T** for hybridization with its fully cDNA sequence. The XPS analysis after hybridization showed an increase of the C1s atomic concentration to 41.4% but also a drop in the N1s peak to 3.47%. The unexpected decrease of the N1s value can be explained by a change of the conformation of the DNA upon hybridization. The resulting DNA double strand adopts a straight conformation due to increased electrostatic interstrand repulsion compared to the single strand, which probably resulted in screening of the nitrogen atoms inside the duplex. Dehybridization of the duplex DNA with double-distilled water (DDW) led to a decrease of the atomic concentration values of C1s and N1s to 35.01% and 2.31%, respectively (Figure 4A,B). Additionally, we have conducted XPS measurements taking into account the atomic concentrations of P (Table 1). Although the atomic concentrations of P are relatively low in comparison to the other measured atoms, it reveals informative data regarding the insertion of the DNA strands into the hydrophobic monolayer. It is clearly evident that the atomic concentrations of P are in correlation with the atomic concentrations of N, further supporting the different stages in which the lipid−DNA molecules were inserted, hybridized, and released from the monolayer.

Notably, all SAM samples were analyzed by XPS at a shallow take-off angle of 23°. The maximum layer thickness is obtained at an angle of 90° with a depth of about 100 Å. As the angle decreases, information is collected from a depth lesser than 100 Å. In accordance, several examples from the literature show conformational changes occurring upon hybridization of immobilized ssDNA molecules.[58−66] Our results further support these observations and interpretations done by other groups. Generally, we claim that the resulting DNA double strand adopts a straight conformation compared to ssDNA. According to Table 1, the Si% and O% decreased upon hybridization, indicating a thicker layer on the surface of the wafer. The N% dropped, where it allegedly was expected to increase, but measurement of the backbone P% revealed similar tendency with a drop in its atomic concentration. We therefore deduce that the duplex DNA adopted a stiff conformation and straightened up, in accordance to previous studies. This change in conformation between shallower ssDNA molecules and the double-stranded (ds) DNA rigid cylinder-like molecules after hybridization may account for the reduction of the measured N% and P% values after hybridization. The XPS measurements performed at a low angle of 23° are sensitive to the DNA-layer thickness changes, which presumably determine the measured atomic composition values.

Confocal fluorescence imaging was used to further confirm the hybridization of the tethered **U4T** with its complementary sequence, here carrying the fluorescent dye label Alexa 488. We observed a characteristic green fluorescence from the **U4T**-modified hydrophobic surface indicative of successful hybridization with the labeled strand (Figure 3A). Already slight washing of the surface with DDW after the presumed formation of the

Table 1. XPS Elemental Analysis (in %)[a]

		chemical modification for the SAM				insertion of **U4T** lipid−DNA						removal of **U4T** lipid−DNA		
		C18			C8:C18 1:8	C18			C8:C18 1:8					
	ref (Si/SiO_2)	1 h*	8 h	48 h	1 h	1 h	8 h	20 h*	20 h	hybridization with **U4T-comp** DNA	dehybridization of **U4T-comp** DNA	ss	ds*	re-insertion of **U4T** lipid−DNA
C	2.39	16.4	28.80	30.56	15.86	32.64	32.74	37.34	40.49	41.19	34.92	27.97	28.14	39.27
N	–	–	–	–	–	3.67	3.61	4.05	4.21	3.47	2.31	2.36	2.26	3.24
O	64.63	53.51	42.97	41.50	54.11	43.02	43.36	39.18	38.03	36.30	38.96	46.04	46.47	38.68
Si	32.97	30.45	28.23	27.94	30.03	20.41	19.74	18.83	17.26	18.50	21.8	23.48	23.13	18.19
P						0.47	0.54	0.61		0.53	0.27	0.16		

[a] The functionalization steps are ordered from left to right according to their chronological order, and those marked with an asterisk were applied for the next step. Briefly, samples were chemically modified with silane derivatives for different time periods; **U4T** lipid−DNA was inserted into the 1 h monolayer, followed by hybridization with cDNA and dehybridization; finally, the lipid−DNA layer was removed by heat treatment either in the ss (before hybridization) or ds (after hybridization) form and new lipid−DNA was re-inserted.

dsDNA led to a significant reduction in fluorescence, as indicated by the decrease in the gray-scale intensity (Figure 3B). On the other hand, hybridization with Alexa 488-labeled non-complementary control DNA resulted in poor fluorescence, demonstrating negligible non-specific absorption to the hydrophobic surface. Fluorescence images were prepared once more, only this time with the lipophilic **U4T** DNA biolayer in a micropattern of squares and lines, in a manner similar to the samples prepared for the AFM measurements (Figure 3C). Images undoubtedly show that lipid−DNA was indeed pierced into the hydrophobic micropattern and underwent hybridization with its complementary fluorescently labeled DNA sequence only in square and line areas.

Moreover, the monolayers with inserted lipid−DNA show high stability, as revealed by extensive washing of the surfaces with water and buffer solutions for periods of up to 48 h. No degradation of the C1s and N1s atomic concentrations was observed at these experimental conditions. Notably, as indicated by XPS results, heating either ss- or ds**U4T**-modified surfaces at temperatures between 80 and 100 °C resulted in removal of the DNA monolayer, leading to recovery of the original hydrophobic monolayer surface (Figure 4A,B). Re-incubation of the heat-treated surface with **U4T** solution showed the same DNA adsorption behavior as described before (compare Figure 2A, B). This process can be repeated for several insertion−heating cycles without any considerable degradation of the hydrophobic monolayer surface and efficiency of insertion. These results have been validated as well by ellipsometry measurements showing a reduction in height after the release of the DNA monolayer to 18.3 ± 0.2 Å (~40% decrease).

All steps depicted in Scheme 1 were also followed using QCM measurements. This method allows probing the functionalization of a piezoelectric crystal with the DNA−lipid sensing interface. More specifically, this method enables the detection of mass changes occurring on the quartz crystal as a result of the hydrophobic monolayer formation, the lipid−DNA insertion, and the hybridization process. Gold-evaporated AT-cut QCM crystals, 9 MHz frequency, were used to follow the formation of octadecylthiol monolayers. A densely packed SAM was detected after ~4 h incubation (Figure 5), as indicated by a saturation plateau and in accordance with literature reports.[55−57] However, a period of 24 h for SAM formation was chosen to ensure that densely packed monolayers are obtained. Using the Sauerbrey equation (eq 1), we calculated a surface density of 2.3×10^{14} molecules/cm^2 upon saturation (a frequency shift of $\Delta H = -22.3$ Hz). This value fits well to the expected surface coverage for similar alkanethiol densely packed monolayers on gold surfaces.

$$\Delta f = -2f_o^2 \frac{\Delta m}{A(\mu_q \rho_q)^{1/2}} \quad (1)$$

Equation 1 expresses the mass change, Δm, occurring on the crystal in terms of crystal frequency change Δ, where f_o is the frequency of the quartz crystal prior to mass change, A is the piezoelectrically active area, ρ_q is the density of quartz (2.648 gr/cm^{-3}), and μ_q is the shear modulus (2.947×10^{11} dyn/cm^{-2} for AT-cut quartz).

The resulting SAM-modified crystals were used as a basis for the insertion of **U2T** and **U4T** lipid−DNAs (both sequences are almost identical, differing only in the number of lipid modifications). Incubation of the QCM crystals in 1 μM solutions of the respective DNA−lipid samples for various periods of time revealed striking differences. In both cases, increasing the incubation time led to further mass increase until a saturation plateau was observed after ~24 h, in accordance with results measured by XPS (curves a and b in Figure 5). The surface density achieved by the insertion of **U4T**-DNA was ~3.8-fold higher than that with **U2T**. This result clearly showed that the more hydrophobic DNA underwent more efficient and stable piercing into the hydrophobic SAM than its less hydrophobic counterpart. These findings suggest the possibility of modulating the insertion or piercing characteristics of lipid−DNA, or biomolecule−lipid hybrids in general, into SAMs by simply engineering their lipophilic nature and the number of lipid−tail anchoring units. As a control, hydrophobic monolayer-modified crystals were incubated in aqueous solutions with 10 μM ODNs, without lipid modification, for similar periods of time. These experiments showed that there is no detectable non-specific adsorption of DNA molecules on the hydrophobic surfaces (curve c in Figure 5), thus demonstrating the need for lipophilic

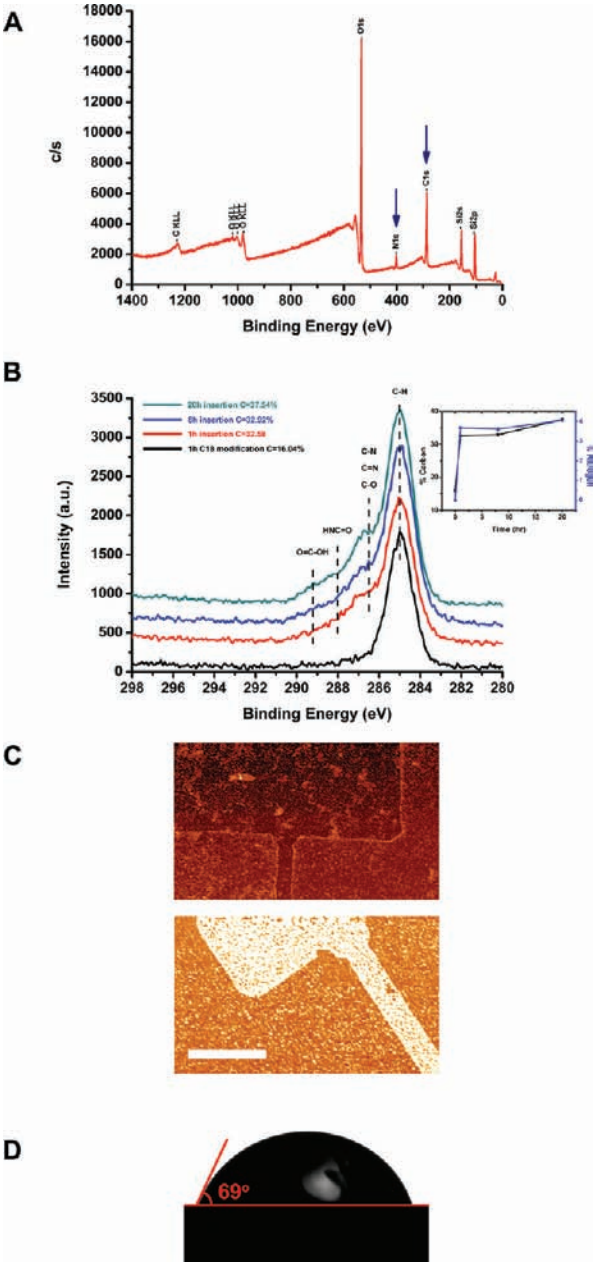

Figure 2. Characterization of the insertion of **U4T** lipid−DNA into the hydrophobic $C_{18}Si$ monolayer. (A) XPS survey spectrum of a 1 h $C_{18}Si$-modified wafer after 20 h incubation with DNA, showing an increase in the C1s peak and the appearance of the N1s peak (marked by arrows) and indicative of successful DNA insertion. (B) High-resolution XPS spectra showing C1s peaks obtained from incubation with **U4T** for 0 (black), 1 (red), 8 (blue), and 20 h (green). Inset: C1s and N1s atomic concentration curves demonstrating a steady increase with time. (C) AFM phase images in a semicontact mode of hydrophobic $C_{18}Si$-micropatterned squares and lines on a hydrophilic SiO_2 wafer before (top) and after (bottom) insertion of **U4T**, indicative of a change in phase with the insertion of the DNA. Scale bar for both images is 16 μm. (D) Contact angle measurements show the reduction of the contact angle value to 69° upon **U4T** insertion.

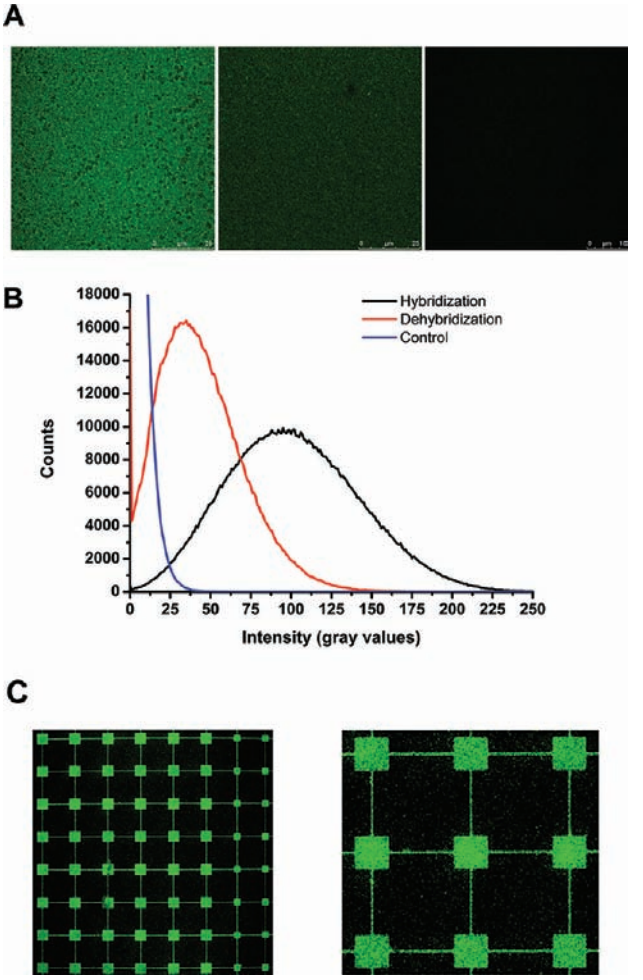

Figure 3. Examination of the hybridization of **U4T-comp** DNA to the anchored **U4T** lipid−DNA. (A) Confocal fluorescent images of silicon wafer modified with $C_{18}Si$ SAM with anchored **U4T**, following hybridization with Alexa 488-labeled **U4T-comp** DNA (left), after a slight wash with DDW (middle), and after hybridization with Alexa-488-labeled control DNA (right). Scale bar is 25 μm for the left and middle images and 10 μm for the right one. (B) A plot of the gray scale intensities calculated from the images in (A), showing a maximum value of 95 for the hybridization with **U4T-comp** and a decrease to a maximum value of 35 after dehybridization of **U4T-comp**, in contrast to almost zero for the non-complementary control DNA. (C) Fluorescence images with the lipophilic **U4T** DNA biolayer in a micropattern of squares and lines, prepared in a similar manner as the samples in (A), after hybridization with its cDNA sequence.

units in order to undergo insertion and anchoring onto the modified solid surface.

Hybridization of the DNA-modified surface with the cDNA target molecules (concentration 1 μM) led to clear mass changes as well. From those data, 62% hybridization efficiency was calculated, equivalent to 1.79×10^{12} molecules/cm^2 of complementary target DNA. On the other hand, hybridization in the presence of non-complementary DNA did not result in any detectable frequency changes. In addition, incubation of the DNA-functionalized QCM crystal in buffer solution at a temperature of 80 °C led to the removal of inserted DNA molecules, in accordance with XPS and ellipsometry measurements.

In order to improve the efficiency of the lipid−DNA insertion process, we investigated the influence of mixed SAMs containing both octadecanethiol ($C_{18}S$) and octanethiol (C_8S) on the surface coverage of the lipid−DNA.

dx.doi.org/10.1021/ja206639d |*J. Am. Chem. Soc.* 2012, 134, 280–292

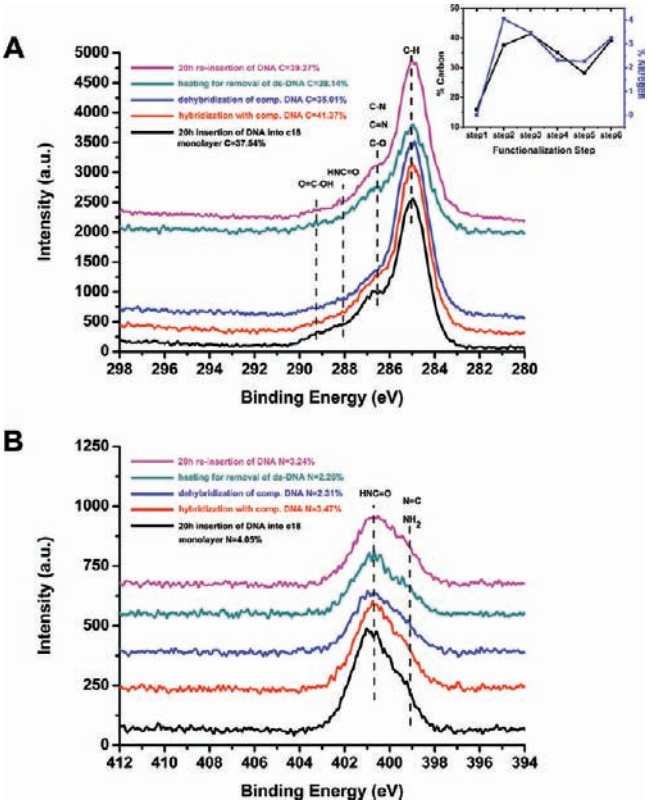

Figure 4. High-resolution XPS spectra of a complete cycle of functionalization and regeneration of a **U4T** lipid−DNA layer. C1s (A) and N1s (B) peaks clearly allow following all the stages of the surface modifications (bottom to top), starting from the increase of the C1s and appearance of the N1s peaks upon non-covalent anchoring of the **U4T** lipid−DNA (black). Next, the selective hybridization of the tethered lipid−DNA with its complement (red) results in a further increase in the C1s peak and a decrease in the N1s peak, whereas dehybridization (blue) leads to a decrease of C1s and a further decrease of N1s. Finally, heating the sample to release the anchored lipid−DNA from the hydrophobic monolayer (green) results in a significant decrease in C1s and N1s values, while re-modification with repeated incubation with **U4T** (pink) induces an increase once more of C1s and N1s values. Inset: C1s and N1s curves showing the relative changes during the functionalization steps: $C_{18}Si$ modification (1), **U4T** lipid−DNA insertion (2), hybridization (3), dehybridization (4), heating (5), and DNA re-insertion (6).

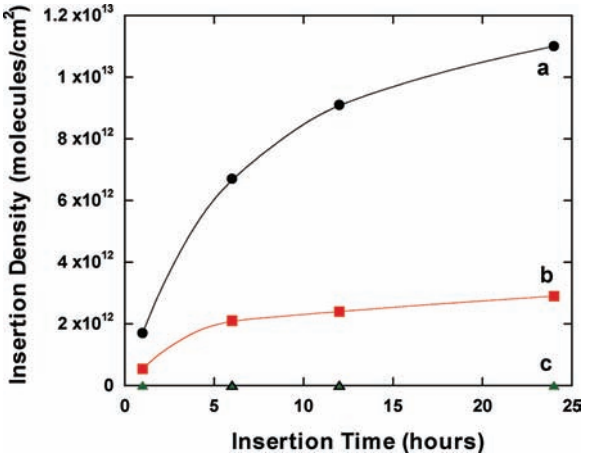

Figure 5. Insertion of lipid−DNA into SAMs measured by QCM. Increasing the incubation time of **U4T** (a) and **U2T** (b) leads to mass increase, until a saturation plateau is observed after ~24 h. Control experiments (c) with 10 μM oligonucleotides without lipid-modification for similar incubation times show that there is no detectable non-specific adsorption of DNA molecules on the hydrophobic surface.

Scheme 2. General Schematic of Mixed SAMs of Octadecanethiol ($C_{18}S$) and Octanethiol (C_8S) Containing Dimension-Controlled Molecular "Pinholes" with a Depth of 10 Carbon Atoms and Anchoring of Lipid−DNA

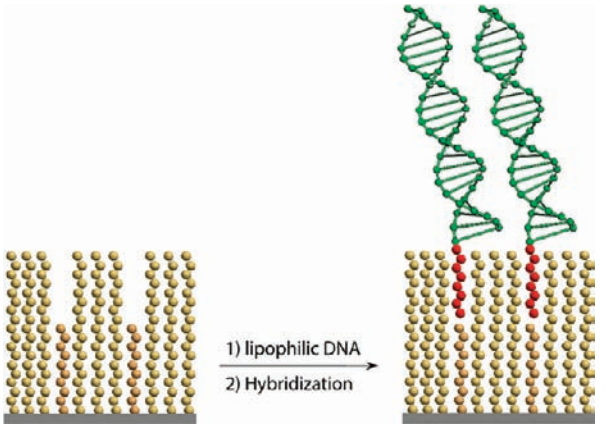

The self-assembly process of C_8S and $C_{18}S$ derivatives is anticipated to create mixed monolayers containing dimension-controlled "defects" with a depth of 10 carbon atoms (the length difference between the alkanethiols, Scheme 2). These engineered "pinholes" are waiting to be filled by the lipophilic tails of the lipid−DNA molecules in order to stabilize the monolayer structure. The lipid−DNA insertion completes the monolayer by filling the gaps, and thus improves the efficiency of the insertion process. A comparison between measurements on 1:8 $C_8S/C_{18}S$, 1:16 $C_8S/C_{18}S$, and $C_{18}S$-only surfaces is presented in Figure 6A for the insertion of **U4T** after 24 h incubation time. These results were further supported by XPS data exhibiting a higher C1s atomic concentration for the insertion of **U4T** into a surface modified with 1:8 $C_8Si/C_{18}Si$ than for insertion into a $C_{18}Si$-only SAM (Figure 6B). The lipid−DNA surface density measured after incubation of these substrates in a 1 μM **U4T** solution was 1.3×10^{13}, 7.5×10^{12}, and 2.5×10^{12} molecules/cm^2 for $C_{18}S$-only, 1:8 $C_8S/C_{18}S$, and 1:16 $C_8S/C_{18}S$ monolayers, respectively. Clearly, the introduction of engineered pinholes into the mixed SAM led to increased insertion efficiency, and this novel strategy may be generally suitable for the improved and controlled fabrication of biomolecule-functionalized surfaces employing biomolecule−lipid hybrids.

Finally, we applied the novel procedure for the non-covalent anchoring of DNA molecules on solid substrates in a sensing setup using a silicon-nanowire (NW) FET device arrays. Semiconducting NWs are emerging as powerful building blocks in nanoscience with the potential to have a significant impact on numerous areas of science and technology.[67−69] In particular, biological sensors based on NW FETs are one of the most promising applications in nanobiotechnology and biomedicine.[70] These devices overcome limitations of planar FET configurations by their 1-D nanoscale morphology, because the extremely high surface-to-volume ratios associated with these nanostructures make their electrical properties extremely sensitive to

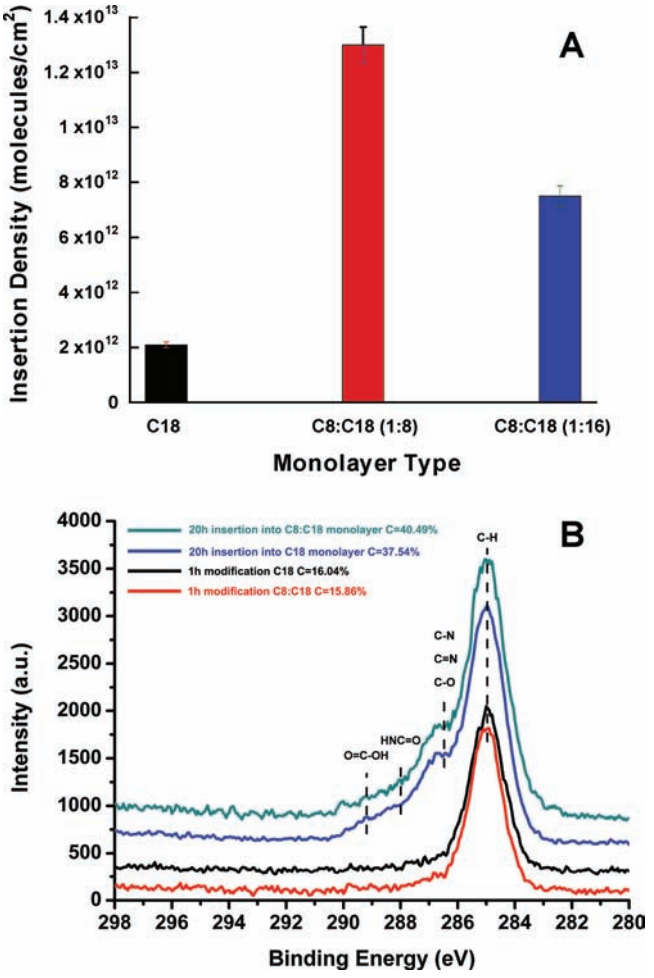

Figure 6. Influence of mixed SAMs on the efficiency of the lipid−DNA insertion process. (A) A comparison of QCM measurements done on 1:8 C_8−C_{18}, 1:16 C_8−C_{18}, and C_{18}-only surfaces. (B) High-resolution XPS spectra showing similar C1s peaks for the formation of hydrophobic monolayers at 1 h incubation with C_{18}Si derivative (black) or mixed C_8Si:C_{18}Si derivatives at ratio of 1:8 (red). However, the C1s peaks for the insertion of the **U4T** reveal higher atomic concentrations obtained for insertion into the mixed C_8Si:C_{18}Si monolayer (green) than into the C_{18}Si monolayer (blue).

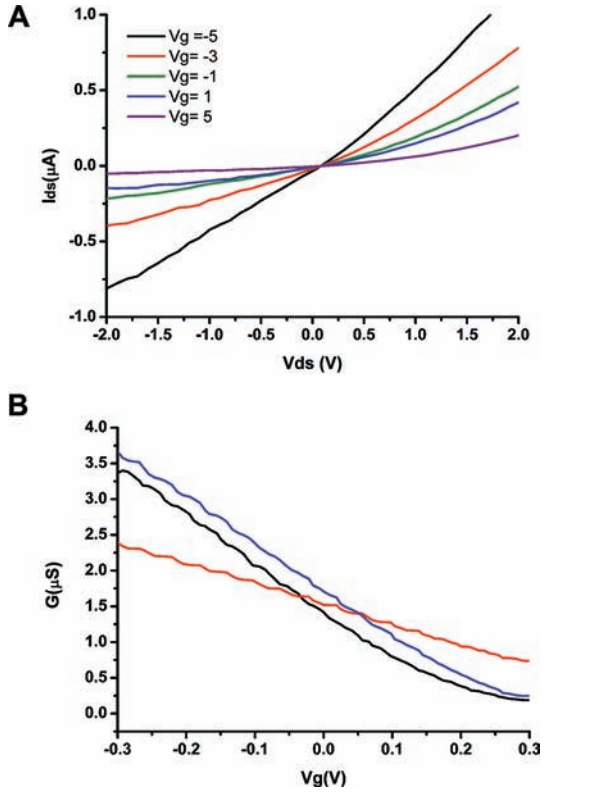

Figure 7. (A) Series of source−drain current (I_{ds}) versus source−drain voltage (V_{ds}) plots at different gate voltages for a typical p-type Si-NW device in air. The black, red, green, blue, and purple curves correspond to gate voltages (V_g) of −5, −3, −1, 1, and 5 V, respectively. (B) Plot of the dependence of the drain−source conductance on the gate voltage curves, demonstrating the response of the same p-type Si-NW FET device at V_{ds} = 0.1 V in solution before DNA insertion into the hydrophobic monolayer (blue), after **U4T** insertion (red), and after the removal of the **U4T** by heat treatment (black).

species adsorbed on their surfaces, up to the detection of single molecules.[71,72] NW-based FETs are configured as sensing devices for biological and chemical molecules by linking receptor groups or probe molecules to the surface of the NWs.[73,74] The devices rely on detecting changes in the electrical conductance occurring as a result of specific binding of target molecules, such as explosives,[73] ATP,[21] DNAs, or proteins,[75−79] onto the sensing surface.

Here, large-scale arrays of Si-NW FET devices were fabricated on silicon wafers for the sensing of negatively charged DNA target molecules. Our sensor chip was designed to contain close to 200 potential devices that can perform simultaneous detection. The signal transduction mechanism does not require labeling of the target DNA molecules; thus it represents a label-free detection method. Si-NWs have a native oxide coating that is naturally formed by exposure to air, allowing us to chemically modify their surface in a manner similar to the silicon oxide surfaces described above.

First, Si-NW FET devices were chemically modified with C_{18}Si to form the hydrophobic SAM, and **U4T** was noncovalently inserted into the hydrophobic monolayer. Subsequently, the chemical modification of the sensing elements and the electrical transport characteristics of the devices were studied. The dependence of source−drain current (I_{SD}) on source−drain voltage (V_{SD}) for varying gate−drain voltages (V_{GD}) for a representative device before any chemical modification is shown in Figure 7A. To assess the efficacy of this system for the sensing of DNA molecules, hybridization buffer (HB) solutions containing various concentrations of fully complementary **U4T** target DNA (**U4T-comp**, 5′-GAATCCGCAAAA-3′), a single-base mismatched cDNA (**U2T-comp**, 5′-GAATCCGCCAAA-3′, where the non-matching nucleotide is underscored), or a non-complementary DNA control (**non-comp**, 5′-TAACAGGAT-3′) were delivered to the sensor chip device through a built-in-chip fluid-delivery system. The conductance changes associated with the response amplitudes of the NW biosensors depend on the device transconductance, which represents the device sensitivity. Thus, it was necessary to measure explicit device sensitivity in order to interpret corresponding signals. A calibration method was used to calibrate the electric responses of the NWs that enabled us to significantly suppress device-to-device variation (see Experimental Section).

Examination of the data (Figure 8A) reveals that the conductance of the NWs is sensitive to the presence of the cDNA (**U4T-comp**) at concentrations of 10 and 1 μM, and displays a

dx.doi.org/10.1021/ja206639d | J. Am. Chem. Soc. 2012, 134, 280–292

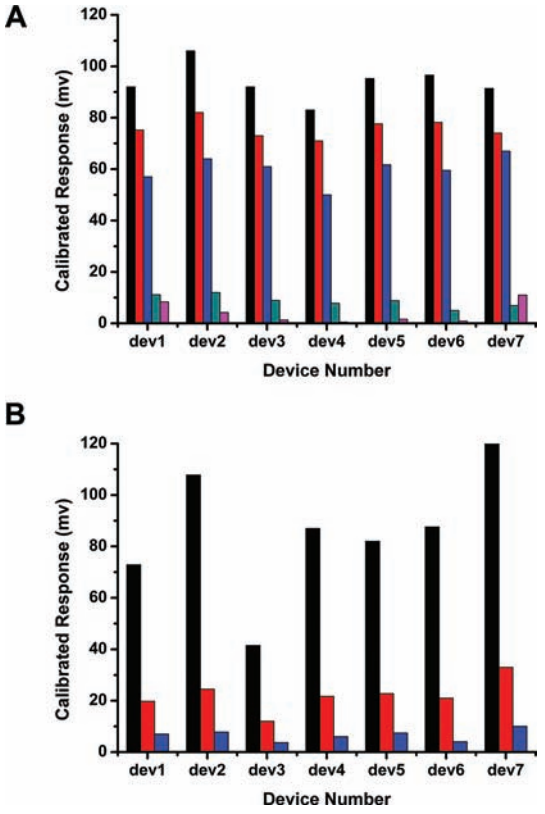

Figure 8. Results of the sensing setup presenting calibrated electrical responses. (A) Comparison of the calibrated responses of seven p-type Si-NW devices functionalized with **U4T** lipid−DNA on the same chip at V_g = −0.2 V, demonstrating the relative difference in the electrical response of the devices upon delivery of 10 μM (black) and 1 μM (red) **U4T**-cDNA; 10 μM (blue) and 1 μM (green) **U2T**-cDNA (with single base mismatch); and 10 μM control DNA strand (magenta) in hybridization buffer solutions. (B) Comparison of the calibrated conductance responses of seven p-type Si-NW devices functionalized with **U4T** lipid−DNA on the same chip at V_g = −0.2 V, following delivery of 10 μM **U4T**-cDNA solution before (black) and after (red) heating the chip to remove the inserted lipid−DNA from the hydrophobic monolayer. In addition, 10 μM control DNA solution was delivered after heating (blue) in order to assess the integrity of the hydrophobic monolayer and the relative non-specific adsorption.

well-defined change in conductance (indicative of hybridization) and subsequent return to baseline (dehybridization) when the cDNA solution and DDW washing solution, respectively, were delivered through the fluid-delivery system to the devices. The change in conductance began immediately upon exposure of the NW devices to **U4T-comp** solution and stabilized at a new value after a few minutes. The DNA sensing was performed also at higher ionic strengths (HB 10 times concentrated), showing similar results (Figure S1). At higher salinity the electrical signal was expected to decrease due to the higher ionic screening; nonetheless, it increased due to more efficient hybridization. Delivery of **non-comp** target molecules at a concentration of 10 μM did not lead to significant changes in the calibrated response of the devices. Furthermore, the specificity of the Si-NW arrays for the detection of target DNA was probed by introducing a single base mismatch sequence (**U2T-comp**). It was found that Si-NW FET devices offer high discrimination for single point mutations (Figure 8A). These results clearly showed the intrinsic selectivity of the DNA recognition layers produced by hydrophobic SAMs and lipid−DNAs. Furthermore, we were able to detect signals in a lower concentration range (Figure S2). For the U4T sequence we tested our devices in a concentration range from 1 fM to 10 μM for the complementary sequence. These experiments resulted in a lower detection limit of 1 pM (s/n ∼3), although sub-picomolar concentrations could still be clearly discerned. Preliminary experiments with a longer capturing DNA sequence (18mer with four hydrophobic 5′-terminal nucleotides) led to a 10-fold higher sensitivity at the relatively high ionic strengths used in our studies (data not shown).

A key factor when considering a real-time field effect sensor is its ability to be quickly regenerated after operation. This feature was successfully realized here as well. After hybridization, washing with only hybridization buffer did not cause any change in conductance, but when DDW washing solution was introduced into the system the device responded rapidly (∼5 min) and the conductance returned to its baseline value (Figure S3).

In addition, we demonstrated the renewable use of our device sensor by simply heating the DNA-inserted monolayer surfaces at temperatures of 80 −100 °C. By this procedure we were able to release the anchored lipid−DNA from the surface, leaving the hydrophobic SAM intact. This process enabled the remodification of the chip with new lipid−DNA probes and recycling of the device sensor. The removal of the lipid−DNA was proven by XPS, ellipsometry, and sensing results. In the sensing setup we injected 10 μM DNA analyte (**U4T-comp**) to the device array before and after the heating treatment, obtaining a clear decrease in the calibrated electrical response after the removal of the inserted lipid−DNA (Figure 8B). Though not very significant, the electrical response after the heating treatment was still detectable. This can be explained either by residual lipid−DNA which was not removed completely from the SAM or by nonspecific adsorption of the DNA analyte onto the hydrophobic surface in the absence of lipid−DNA. Re-modification of the Si-NW FET devices with **U4T** was then undertaken, showing a restoration of the electrical response with the injection of the analyte. A plot of the dependence of the drain-source conductance of a single p-type Si-NW FET device on the gate voltage demonstrated a similar response before lipid−DNA insertion into the monolayer and after removal of **U4T** by heat treatment, but different behavior after **U4T** insertion (Figure 7B). The detection of DNA was performed simultaneously by at least 10 NW devices, all demonstrating electrical response when incubated with cDNA.

CONCLUSIONS

In this work we present a novel non-covalent preparation technique for nucleic acid-functionalized surface layers. Likewise, we describe the comprehensive characterization of the biofunctional layer and finally its potential use for sensing applications. lipid−DNA layers were prepared by the insertion of DNA species into dense hydrophobic SAMs. The insertion process took place through the piercing of the lipophilic units of the lipid−DNA into the alkane SAM, as confirmed by XPS, QCM, contact angle, elipsometry, AFM, and confocal imaging measurements. Such DNA layers can be readily formed on metal and semiconductor surfaces, both showing similar insertion efficiencies. Furthermore, mixed monolayers were shown to improve the efficiency of the insertion process and increase the resulting DNA surface density. The DNA-inserted layers showed high

hybridization yields with target DNA molecules and insignificant non-specific adsorption of non-complementary sequences. Notably, these anchored DNA−lipid molecule layers could be substantially released through heating at temperatures of 80−100 °C, leaving behind DNA-free lipophilic monolayers ready for additional cycles of lipid−DNA insertion. Finally, this novel DNA surface anchoring process was successfully applied for the selective sensing of DNAs by Si-NW FET device arrays, and their regeneration through heat treatment and re-incubation was demonstrated. Several of the novel approaches described in this article may be readily applied for the non-covalent immobilization of other biomolecular species, such as proteins and antibodies.

EXPERIMENTAL SECTION

Materials. All chemicals were used as purchased without any further purification. The synthesis of lipid−DNAs was described previously.[53,54] At the 5′-ends of both lipid−DNAs, either two (**U2T**: 5′-UUTGGCGGATTC-3′) or four (**U4T**: 5′-UUUUGCGGATTC-3′) hydrophobically modified uridines (U) containing 5-(dodec-1-ynyl)uracil as the nucleobase were installed. The ODN analytes, **U4T-comp** (5′-GAATCCGCAAAA-3′), **U2T-comp** (5′-GAATCCGCCAAA-3′), and control DNA (**non-comp**, 5′-TAACAGGAT-3′), were all purchased from Sigma-Aldrich Inc., both 5′-labeled with Alexa-488 and unlabeled. Octadecylmercaptan and octanethiol were purchased from Sigma-Aldrich Inc. *n*-Octadecyldimethylchlorosilane, *n*-octyldimethylchlorosilane, and (heptadecafluoro)-1,1,2,2-tetrahydrodecyldimethylchlorosilane were purchased from Gelest Inc. Solvents were purchased from Biolab Ltd., Israel, and were used without any further purification. Silicon wafers with 600 nm thermal oxide, SSP prime grade, were obtained from Silicon Quest International. QCM crystals were purchased from ICM Inc., USA.

Preparation of Self-Assembled Monolayers on Gold-Covered QCM crystals. QCM crystals were modified by incubation on 0.1−2.0 mM ethanolic solution of the respective alkanethiol derivative (thiol solutions were purged with nitrogen before incubation) for a given period of time. The crystals were then thoroughly washed with ethanol and dried under a stream of nitrogen. Crystals were kept under a nitrogen atmosphere until used in the next modification steps.

Preparation of Self-Assembled Hydrophobic Monolayers on Silicon Wafers. Prior to the chemical modification, samples were cleaned with a piranha solution (70% H_2SO_4:30% H_2O_2) for 10 min, followed by oxygen plasma treatment: 100 W and 50 sccm O_2 for 200 s. Cleaned wafers were dehydrated on a 200 °C hot plate for 2 h. Substrates were then modified with 1% (v/v) octadecyldimethylchlorosilane (C_{18}Si) or *n*-octyldimethylchlorosilane (C_8Si) in extra dry *n*-heptane in a sealed cup for 1 h at room temperature, at a clean room with low-humidity atmosphere of about 42%. Samples were immediately rinsed with heptane for 10 min with stirring, followed by a short sonication and intensive wash in acetone. Samples were blown dry with N_2 and left for a curing step at 110 °C for 1 h.

The fluorosilane modification was carried out with 1% 1,1,2,2-tetrahydrodecyldimethylchlorosilane in extra dry DCM/heptane 1:1 solution for 1 h, at a clean room with low-humidity atmosphere. Samples were immediately rinsed with DCM for 1 min, followed by a curing step at 110 °C for 10 min, washed with acetone, and blown dry with N_2.

Insertion of Lipid−DNA Molecules into the Self-Assembled Monolayers. The DNA insertion of **U2T** and **U4T** was performed at room temperature in 10 mM Tris buffer, pH 7.4 (insertion buffer). The lipid−DNA naturally formed micelles above the critical micelle concentration (CMC), which are dynamic and therefore enable individual DNA molecules to exchange between micelles and also anchor their hydrophobic tails into the hydrophobic monolayer. There was no need for heating or sonicating the samples to destabilize the micelles. The CMC values of the used lipid−DNAs have been published previously[54] and are 2.04 and 1.27 μM for **U2T** and **U4T**, respectively. In this work, the concentration of the amphiphilic DNA is kept at <1 μM, which is well below the CMC. Therefore, the presence of micelle structures is unlikely.

Following incubation with the lipid−DNA, samples were thoroughly washed with the insertion buffer.

Hybridization and Dehybridization of the Lipid−DNA Molecules. Hybridization of the lipid−DNAs with the DNA analytes was performed at room temperature in hybridization buffer (10× HB) containing 0.01 M Tris, 0.01 M EDTA, 0.05 M NaCl, pH 7.4, and 10 times diluted HB solution. Dehybridization was performed by sequential washing with copious amounts of DDW. Under these conditions, the melting temperature of **U4T** is around room temperature (Figure S5). It is important to note that preparation of all samples for characterization (i.e., XPS, AFM, contact angle, ellipsometry, and confocal imaging) was performed in a clean room at a temperature of 20 °C. As well, all sensing experiments were conducted at 20 °C in accordance.

Sample Preparation for Characterization by XPS, QCM, Contact Angle, Confocal Microscopy, Ellipsometry, and AFM. *XPS Measurements.* XPS studies were preformed on silicon wafers, using 5600 Multi-Technique System (PHI, USA) with a base pressure of 2.5×10^{-10} Torr. Samples were irradiated with an Al Kα monochromated source (1486.6 eV), and the released electrons were analyzed by a Spherical Capacitor Analyzer using a slit aperture of 0.8 mm. Sample charging was compensated (if required) with a charge neutralizer (C1s at 285 eV was taken as an energy reference). The SAM samples were analyzed on the surface only at a shallow takeoff angle of 23°. High-resolution XPS measurements were taken at pass energy of 11.75 eV with 0.05 eV/step interval.

Preparation of Samples. Briefly, samples were chemically modified as previously described for the formation of the SAM but with different time periods of 1, 8, and 48 h for the chemical modification with C_{18}Si and 1 h for the mixed monolayer of C_8:C_{18}. **U4T** was incubated with the 1 h-reacted C_{18}Si hydrophobic monolayer for time periods of 1, 8, and 20 h and with the mixed C_8:C_{18} monolayer for 20 h. Hybridization with the full complement to **U4T** took place on the 20 h-anchored **U4T** on the C_{18}Si SAM with HB at room temperature. Samples were then washed with HB several times. Dehybridization of dsDNA was realized by extensive washing with DDW. Finally, samples with **U4T**-anchored ss or ds lipid−DNA were heated to 80−100 °C for 10 min for the release of DNA from the hydrophobic surface. Samples were then recycled with **U4T** lipid−DNA that was re-inserted as described above.

QCM Measurements. A home-built QCM analyzer equipped with a Fluke 164T multifunction counter was used for the microgravimetric QCM experiments. Quartz crystals (AT-cut, 9 MHz) sandwiched between two Au electrodes (roughness factor ca. 3.5 with an area of 0.196 cm^2) were used in microgravimetric experiments. Quartz electrodes were cleaned with a piranha solution (70% H_2SO_4:30% H_2O_2) for 15 min, rinsed thoroughly with DDW, and dried with a stream of argon.

Contact Angle Measurements. Contact angle measurements were taken using Ramé-Hart instruments (Dropimage, CA).

Preparation of Samples. Samples were cleaned and chemically modified in a manner similar to that used for the XPS samples as described. Contact angles of water droplets on the C_{18} hydrophobic self-assembled monolayers at different time intervals showed increased values with longer incubation times without significant change after 8 h; angles of 92° and 95° were achieved already after incubation times of 1 and 8 h, respectively, in comparison to a contact angle of ∼42° measured for the pristine silicon substrate. The insertion of **U4T** into the hydrophobic monolayer at different time intervals of 1 and 8 h showed a distinct decrease in the contact angle to values of 70° and 69°, respectively.

These values are indicative for the insertion of the **U4T** lipid−DNA, creating a moderately hydrophilic surface in comparison to the former hydrophobic one.

Confocal Fluorescence Imaging. Confocal fluorescent images were obtained with a Leica SP5 confocal microscope. Images were acquired using excitation at 488 nm and emission range of 500−550 nm with X63 1.4 NA Plan-Apo oil immersion objective using LASAF software.

Preparation of Samples. SAM samples were chemically modified as previously described for XPS measurements for 1 h followed by the insertion of **U4T** lipid−DNA for 20 h and extensive washing with insertion buffer. Next, hybridization with complementary **U4T** Alexa 488-labeled DNA and non-complementary Alexa 488-labeled control DNA were each performed at room temperature. Finally, dehybridization was realized by a slight wash with DDW.

All fluorescence micrographs that were compared regarding their intensity were taken under the very same conditions, on the same day, in order to minimize signal variations between the different samples. Parameters such as pinhole, zoom, illumination, exposure, noise, offset, contrast, etc. were kept fixed.

Thickness Measurements by Ellipsometry. Ellipsometric measurements were carried out on a M-2000DUV spectroscopic ellipsometer (J.A. Woollam Co., Inc.). The angles of incidence were 65°, 70°, and 75°, with a spot size of 2−3 mm. The data were analyzed using WVASE32 software installed with the ellipsometer. The film thicknesses of the examined monolayers were calculated by using the Cauchy model.

Preparation of Samples. Samples were treated as previously described on wafers of 100 nm thermal oxide, with the same sample measured after each functionalization step.

Atomic Force Microscopy. Images were taken in a tapping mode using an Agilent 5500 SPM atomic force microscope and a probe of NSC18/AIBS of μ-masch with a spring constant of 3.5 N/m. Data for the two images were recorded sequentially using a phase image signal source.

Preparation of Samples. A lipophilic **U4T** biolayer micropattern of squares and lines was created. First, a pattern of squares and lines was formed on a clean silcon wafer by photolithography. Next, chemical modification with $C_{18}Si$ was performed as previously described for 1 h, followed immediately by removal of the photoresist by brief sonication and sequential washing with acetone, resulting in hydrophobic micropattern on the hydrophilic silicon wafer. **U4T** lipid−DNA was inserted into the hydrophobic monolayer for 20 h by fully covering the substrate with solution, followed by extensive washing with insertion buffer. The geometry of the pattern undoubtedly showed a marked phase shift across the boundaries, indicative of the change in phase from the hydrophobic C_{18} pattern to a more hydrophilic one with the insertion of the lipid−DNA into the pattern.

Si-NWs Synthesis, Device Array Fabrication, Sensing, and Electrical Characterization. *Si-NWs Synthesis.* Silicon nanowires were synthesized by chemical vapor deposition as previously described.[80] In short, 20 nm gold nanoparticles (Ted Pella), which served as catalyst sites for the VLS-CVD growth of Si-NWs, were initially deposited on Si (100) growth substrates. To promote the adhesion of the gold nanoparticles to the silicon substrate, a poly-L-lysine solution (Ted Pella) was applied to the bare silicon wafer, as an electrostatic binding agent. The nanoparticle-decorated wafer was then placed in a horizontal tube furnace for the growth of the Si-NWs. Silane and diborane were used as reactants during the growth to provide boron as a p-type dopant with a B:Si ratio of 1:4000.

Nanowire FET Fabrication. Si-NW FET devices were fabricated by photolithography. Briefly, source and drain electrodes were deposited with the use of a multilayer photoresist structure consisting of 300 nm LOR3A (Microchem) and 500 nm 1805 (Shipley). After exposure and development of the electrode patterns, the contacts were metallized by e-beam and thermal evaporation of Ti/Pd/Ti (2/60/8 nm), respectively, and were then passivated from the electrolyte with an insulating layer of Si_3N_4 (100 nm thick) deposited by plasma-enhanced chemical vapor deposition. The separation between the source and drain electrodes for each FET was 2 μm.

Fluid-Delivery System. The fluid-delivery system was fabricated from flexible polydimethylsiloxane (PDMS) elastomer mixed in a 10:1 ratio with base as curing agent. The PDMS was cured overnight in an oven at 60 °C and then cut into rectangular pieces. The dimensions of the PDMS were 10 × 10 × 5 mm.

Data Acquisition, Electrical Setup, and Sensing. The basic electrical properties of the Si-NW devices on the sensor chip were first characterized in air as this provides means for quality control before completion of the sensor structure. The sensor device chip was then integrated with a custom-made PDMS microfluidic channel and wire bonded to the outside conductive pads for the electrical measurements. The conductance of the Si-NW FET was measured by application of AC bias (70 kHz, 100 mV) by means of a lock-in amplifier (Stanford Research System model SR830 DSP). The drain current was amplified with a variable-gain amplifier (model 99539 Amplifier System) and filtered by the lock-in amplifier with a time-constant setting of 300 ms. The output data were recorded by using a multichannel I/O adaptor panel (BNC-2090, National Instrument). DNA sensing studies were carried out by monitoring the conductance of the Si-NW devices over time while DNA analytes were delivered to the sensing chip by the microfluidic system using a syringe pump (Dolomite Mitos Syringe Pump XS) at a flow rate of 5 μL/min. The action of injecting the solution might introduce some negligible noise into the electrical read-out signal. All studies were carried out at room temperature.

Calibration of Device Responses. The calibration technique is based on correlating between the NW gate dependence (dI_{ds}/dV_g) and the absolute response (absolute change in current, ΔI).[81] The absolute response was divided by (dI_{ds}/dV_g) for each device, which significantly improved the device to device variation, as verified by a decrease in the coefficient of variation (CV). The CV is defined as the ratio of the standard deviation σ to the mean μ as described by the equation CV = σ/μ.

■ ASSOCIATED CONTENT

Supporting Information. Figure S1, comparison of Si-NW FET sensitivities at different ionic strengths; Figure S2, typical concentration-dependent sensing results using lipid−DNA functionalized surfaces; Figure S3, representative real-time sensing experiments using Si-NWs FETs; Figure S4, contact angle measurements of a fluorosilane derivative monolayer on silicon surfaces; Figure S5, T_m analysis, performed by UV spectroscopy, of **U4T**; Figure S6, anion-exchange chromatograms of the purified lipid−DNAs, **U2T**, and **U4T**. This material is available free of charge via the Internet at http://pubs.acs.org.

■ AUTHOR INFORMATION

Corresponding Author

fernando@post.tau.ac.il; a.herrmann@rug.nl

Author Contributions

[#]These authors contributed equally to this work.

■ ACKNOWLEDGMENT

We thank the Legacy Foundation and Israel Science Foundation for financial support. We thank Dr. Leonid Mittelman for his professional assistance with confocal microscope experiments. M.K. and A.H. were supported by the EU (ERC starting grant, ECCell), the Netherlands Organization for Scientific Research

(NWO-Vici), the German Research Foundation, and the Zernike Institute for Advanced Materials.

REFERENCES

(1) Chen, K.-I.; Li, B.-R.; Chen, Y.-T. *Nano Today* **2011**, *6*, 131.
(2) Kasemo, B. *Surf. Sci.* **2002**, *500*, 656.
(3) Cattani-Scholz, A.; Pedone, D.; Blobner, F.; Abstreiter, G.; Schwartz, J.; Tornow, M.; Andruzzi, L. *Biomacromolecules* **2009**, *10*, 489.
(4) Ray, S.; Mehta, G.; Srivastava, S. *J. Proteom.* **2010**, *10*, 731.
(5) Stutzmann, M.; Garrido, J. A.; Eickhoff, M.; Brandt, M. S. *Phys. Status Solidi A* **2006**, *203*, 3424.
(6) Li, H.; Carter, J. D.; LaBean, T. H. *Mater. Today.* **2009**, *12*, 24.
(7) Chow, D. C.; Johannes, M. S.; Lee, W.-K.; Clark, R. L.; Zauscher, S.; Chilkoti, A. *Mater. Today.* **2005**, *8*, 30.
(8) He, Y.; Su, S.; Xu, T.; Zhong, Y.; Zapien, J. A.; Li, J.; Fan, C.; Lee, S.-T. *Nano Today.* **2011**, *6*, 122.
(9) Socher, E.; Bethge, L.; Knoll, A.; Jungnick, N.; Herrmann, A.; Seitz, O. *Angew. Chem., Int. Ed.* **2008**, *47*, 9555.
(10) Mallouk, T. E.; Yang, P. *J. Am. Chem. Soc.* **2009**, *131*, 7937.
(11) Weizmann, Y.; Chenoweth, D. M.; Swager, T. M. *J. Am. Chem. Soc.* **2011**, *133*, 3238.
(12) He, Y.; Fan, C.; Lee, S.-T. *Nano Today.* **2010**, *5*, 282.
(13) Roy, S.; Gao, Z. *Nano Today.* **2009**, *4*, 318.
(14) Yang, P.; Yan, R.; Fardy, M. *Nano Lett.* **2010**, *10*, 1529.
(15) Peelle, B. R.; Krauland, E. M.; Wittrup, K. D.; Belcher, A. M. *Acta Biomater.* **2005**, *1*, 145.
(16) Kang, J.; Loew, M.; Arbuzova, A.; Andreou, I.; Dähne, L. *Adv. Mater.* **2010**, *22*, 3548.
(17) Curreli, M.; Li, C.; Sun, Y.; Lei, B.; Gundersen, M. A.; Thompson, M. E.; Zhou, C. *J. Am. Chem. Soc.* **2005**, *127*, 6922.
(18) Wang, J.; Liu, G.; Jan, M. R. *J. Am. Chem. Soc.* **2004**, *126*, 3010.
(19) Star, A.; Tu, E.; Niemann, J.; Gabriel, J.-C. P.; Joiner, C. S.; Valcke, C. *Proc. Natl. Acad. Sci. U.S.A.* **2006**, *103*, 921.
(20) Weizmann, Y.; Chenoweth, D. M.; Swager, T. M. *J. Am. Chem. Soc.* **2010**, *132*, 14009.
(21) Patolsky, F.; Zheng, G.; Lieber, C. M. *Anal. Chem.* **2006**, *78*, 4260.
(22) Patolsky, F.; Zheng, G.; Lieber, C. M. *Nanomed.* **2006**, *1*, 51.
(23) Wu, Y.; Xiang, J.; Yang, C.; Lu, W.; Lieber, C. M. *Nature* **2004**, *430*, 61.
(24) Weizmann, Y.; Elnathan, R.; Lioubashevski, O.; Willner, I. *Nano Lett.* **2005**, *5*, 741.
(25) Prigodich, A. E.; Lee, O.-S.; Daniel, W. L.; Seferos, D. S.; Schatz, G. C.; Mirkin, C. A. *J. Am. Chem. Soc.* **2010**, *132*, 10638.
(26) Macfarlane, R. J.; Lee, B.; Hill, H. D.; Senesi, A. J.; Seifert, S.; Mirkin, C. A. *Proc. Natl. Acad. Sci. U.S.A.* **2009**, *106*, 10493.
(27) Weizmann, Y.; Elnathan, R.; Lioubashevski, O.; Willner, I. *J. Am. Chem. Soc.* **2005**, *127*, 12666.
(28) Kelley, S. O.; Boon, E. M.; Barton, J. K.; Jackson, N. M.; Hill, M. G. *Nucleic Acids Res.* **1999**, *27*, 4830.
(29) Kang, T.; Yoo, S. M.; Yoon, I.; Lee, S. Y.; Kim, B. *Nano Lett.* **2010**, *10*, 1189.
(30) Slinker, J. D.; Muren, N. B.; Gorodetsky, A. A.; Barton, J. K. *J. Am. Chem. Soc.* **2010**, *132*, 2769.
(31) Slinker, J. D.; Muren, N. B.; Renfrew, S. E.; Barton, J. K. *Nat. Chem* **2011**, *3*, 228.
(32) Stoeva, S. I.; Lee, J.-S.; Thaxton, C. S.; Mirkin, C. A. *Angew. Chem., Int. Ed.* **2006**, *45*, 3303.
(33) Chow, D. C.; Lee, W.-K.; Zauscher, S.; Chilkoti, A. *J. Am. Chem. Soc.* **2005**, *127*, 14122.
(34) Wang, X.; Ozkan, C. S. *Nano Lett.* **2008**, *8*, 398.
(35) Li, Z.; Chen, Y.; Li, X.; Kamins, T. I.; Nauka, K.; Williams, R. S. *Nano Lett.* **2004**, *4*, 245.
(36) Zhou, D.; Ying, L.; Hong, X.; Hall, E. A.; Abell, C.; Klenerman, D. *Langmuir* **2008**, *24*, 1659.
(37) Zhang, G.-J.; Zhang, G.; Chua, J. H.; Chee, R.-E.; Wong, E. H.; Agarwal, A.; Buddharaju, K. D.; Singh, N.; Gao, Z.; Balasubramanian, N. *Nano Lett.* **2008**, *8*, 1066.
(38) Jiang, G.; Susha, A. S.; Lutich, A. A.; Stefani, F. D.; Feldmann, J.; Rogach, A. L. *ACS Nano* **2009**, *3*, 4127.
(39) Ingebrandt, S.; Offenhäusser, A. *Phys. Status Solidi A* **2006**, *203*, 3399.
(40) Erokhina, S.; Berzina, T.; Cristofolini, L.; Konovalov, O.; Erokhin, V.; Fontana, M. P. *Langmuir* **2007**, *23*, 4414.
(41) Kotzabasakis, V.; Georgopoulou, E.; Pitsikalis, M.; Hadjichristidis, N.; Papadogianakis, G. *J. Mol. Catal. A: Chem.* **2005**, *231*, 93.
(42) Kakizawa, Y.; Kataoka, K. *Adv. Drug Delivery Rev.* **2002**, *54*, 203.
(43) Kataoka, K.; Harada, A.; Nagasaki, Y. *Adv. Drug Delivery Rev.* **2001**, *47*, 113.
(44) Savić, R.; Luo, L.; Eisenberg, A.; Maysinger, D. *Science* **2003**, *300*, 615.
(45) Ding, K.; Alemdaroglu, F. E.; Börsch, M.; Berger, R.; Herrmann, A. *Angew. Chem., Int. Ed.* **2007**, *46*, 1172.
(46) Alemdaroglu, F. E.; Ding, K.; Berger, R.; Herrmann, A. *Angew. Chem., Int. Ed.* **2006**, *45*, 4206.
(47) Li, Z.; Zhang, Y.; Fullhart, P.; Mirkin, C. A. *Nano Lett.* **2004**, *4*, 1055.
(48) Jeong, J. H.; Park, T. G. *Bioconjugate Chem.* **2001**, *12*, 917.
(49) Gore, T.; Dori, Y.; Talmon, Y.; Tirrell, M.; Bianco-Peled, H. *Langmuir* **2001**, *17*, 5352.
(50) Yu, Y.-C.; Berndt, P.; Tirrell, M.; Fields, G. B. *J. Am. Chem. Soc.* **1996**, *118*, 12515.
(51) Pfeiffer, I.; Höök, F. *J. Am. Chem. Soc.* **2004**, *126*, 10224.
(52) Chan, Y.-H. M.; van Lengerich, B.; Boxer, S. G. *Proc. Natl. Acad. Sci. U.S.A.* **2009**, *106*, 979.
(53) Kwak, M.; Minten, I. J.; Anaya, D.-M.; Musser, A. J.; Brasch, M.; Nolte, R. J. M.; Müllen, K.; Cornelissen, J. J. L. M.; Herrmann, A. *J. Am. Chem. Soc.* **2010**, *132*, 7834.
(54) Anaya, M.; Kwak, M.; Musser, A. J.; Müllen, K.; Herrmann, A. *Chem.—Eur. J* **2010**, *16*, 12852.
(55) Baralia, G. G.; Duwez, A. S.; Nysten, B.; Jonas, A. M. *Langmuir* **2005**, *21*, 6825.
(56) Collard, D. M.; Fox, M. A. *Langmuir* **1991**, *7*, 1192.
(57) Chen, L. J. *J. Mater. Chem.* **2007**, *17*, 4639.
(58) Fritz, J.; Baller, M. K.; Lang, H. P.; Rothuizen, H.; Vettiger, P.; Meyer, E.-J.; Güntherodt, H.; Gerber, C.; Gimzewski, J. K. *Science* **2000**, *288*, 316.
(59) Ilic, B.; Yang, Y.; Aubin, K.; Reichenbach, R.; Krylov, S.; Craighead, H. G. *Nano Lett.* **2005**, *5*, 925.
(60) Sinensky, A. K.; Belcher, A. M. *Nat. Nanotechnol.* **2007**, *2*, 653.
(61) Mertens, J.; Rogero, C.; Calleja, M.; Ramos, D.; Martin-Gago, J. A.; Briones, C.; Tamayo, J. *Nat. Nanotechnol.* **2008**, *3*, 301.
(62) Levicky, R.; Herne, T. M.; Tarlov, M. J.; Satija, S. K. *J. Am. Chem. Soc.* **1998**, *120*, 9787.
(63) Krishnan, Y.; Simmel, F. C. *Angew. Chem., Int. Ed.* **2011**, *50*, 3124.
(64) Poghossian, A.; Cherstvy, A.; Ingebrandt, S.; Offenhäusser, A.; Schöning, M. J. *Sens. Actuators, B.* **2005**, *111*, 470.
(65) Gębala, M.; Schuhmann, W. *ChemPhysChem.* **2010**, *11*, 2887.
(66) Husale, S.; Persson, H. H. J.; Sahin, O. *Nature* **2009**, *462*, 1075.
(67) Kim, W.; Ng, J. K.; Kunitake, M. E.; Conklin, B. R.; Yang, P. *J. Am. Chem. Soc.* **2007**, *129*, 7228.
(68) Yang, P. *MRS Bull.* **2005**, *30*, 85.
(69) Tian, R.; Regonda, S.; Gao, J.; Liu, Y.; Hu, W. *Lab Chip* **2011**, *11*, 1952.
(70) Stern, E.; Steenblock, E. R.; Reed, M. A.; Fahmy, T. M. *Nano Lett.* **2008**, *8*, 3310.
(71) Stern, E.; Wagner, R.; Sigworth, F. J.; Breaker, R.; Fahmy, T. M.; Reed, M. A. *Nano Lett.* **2007**, *7*, 3405.
(72) Patolsky, F.; Zheng, G.; Hayden, O.; Lakadamyali, M.; Zhuang, X.; Lieber, C. M. *Proc. Natl. Acad. Sci. U.S.A.* **2004**, *101*, 14017.
(73) Elibol, O. H.; Morisette, D.; Akin, D.; Denton, J. P.; Bashir, R. *App. Phys. Lett.* **2003**, *83*, 4613.
(74) Stern, E.; Klemic, J. F.; Routenberg, D. A.; Wyrembak, P. N.; Turner-Evans, D. B.; Hamilton, A. D.; LaVan, D. A.; Fahmy, T. M.; Reed, M. A. *Nature* **2007**, *445*, 519.

(75) Engel, Y.; Elnathan, R.; Pevzner, A.; Davidi, G.; Flaxer, E.; Patolsky, F. *Angew. Chem., Int. Ed.* **2010**, *122*, 6835.
(76) Stern, E.; Vacic, A.; Reed, M. A. *IEEE Trans. Electron Devices* **2008**, *55*, 3119.
(77) Zheng, G.; Patolsky, F.; Cui, Y.; Wang, W. U.; Lieber, C. M. *Nat. Biotechnol.* **2005**, *23*, 1294.
(78) Timko, B. P.; Cohen-Karni, T.; Yu, G.; Qing, Q.; Tian, B.; Lieber, C. M. *Nano Lett.* **2009**, *9*, 914.
(79) Wang, W. U.; Chen, C.; Lin, K.-h.; Fang, Y.; Lieber, C. M. *Proc. Natl. Acad. Sci. U.S.A.* **2005**, *102*, 3208.
(80) Patolsky, F.; Zheng, G.; Lieber, C. M. *Nat. Protocols* **2006**, *1*, 1711.
(81) Ishikawa, F. N.; Curreli, M.; Chang, H.-K.; Chen, P.-C.; Zhang, R.; Cote, R. J.; Thompson, M. E.; Zhou, C. *ACS Nano* **2009**, *3*, 3969.